

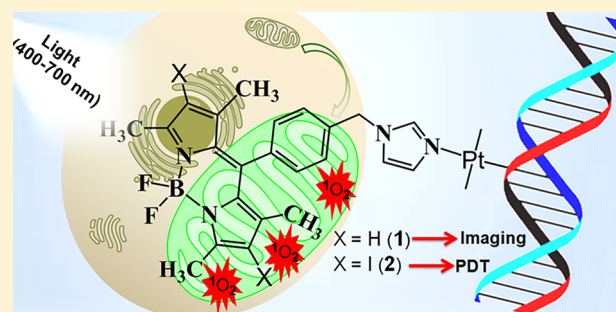
# Monofunctional BODIPY-Appended Imidazoplatin for Cellular Imaging and Mitochondria-Targeted Photocytotoxicity

Md Kausar Raza,<sup>†</sup> Srishti Gautam,<sup>‡</sup> Aditya Garai,<sup>†</sup> Koushambi Mitra,<sup>†</sup> Paturu Kondaiah,<sup>\*,‡</sup> and Akhil R. Chakravarty<sup>\*,†</sup>

<sup>†</sup>Department of Inorganic and Physical Chemistry and <sup>‡</sup>Department of Molecular Reproduction, Development and Genetics, Indian Institute of Science, Bangalore 560012, India

## Supporting Information

**ABSTRACT:** Monofunctional platinum(II) complexes of formulation  $cis-[Pt(NH_3)_2(L)Cl](NO_3)$ , where L is an imidazole base conjugated to 4,4-difluoro-4-bora-3a,4a-diaza-s-indacene (BODIPY) with emissive ( $L^1$  in **1**) and nonemissive ( $L^2$  in **2**) moieties were prepared and characterized, and their singlet oxygen-mediated photoinduced cytotoxicity was studied. The 1-methylimidazole (1-MeIm) complex **3** was prepared as a control and for structural characterization by X-ray crystallography. Complexes **1** and **2** showed strong visible absorption bands at 500 nm ( $\epsilon = 2.7 \times 10^4 \text{ M}^{-1} \text{ cm}^{-1}$ ) and 540 nm ( $1.4 \times 10^4 \text{ M}^{-1} \text{ cm}^{-1}$ ). Complex **1** is emissive with a band at 510 nm ( $\Phi_F = 0.09$ ) in 1% dimethyl sulfoxide/Dulbecco's Modified Eagle's Medium (pH 7.2). Singlet oxygen generation upon photoirradiation with visible light (400–700 nm) was evidenced from 1,3-diphenylisobenzofuran titration experiments showing significant photosensitizing ability of the BODIPY complexes. Both **1** and **2** were remarkably photocytotoxic in visible light (400–700 nm,  $10 \text{ J cm}^{-2}$ ) in skin keratinocyte HaCaT and breast cancer MCF-7 cells giving  $IC_{50}$  values in nanomolar concentration. The complexes were, however, essentially nontoxic to the cells in the dark ( $IC_{50} > 80 \mu\text{M}$ ). Complex **2** having a diiodo-BODIPY unit is nonemissive but an efficient photosensitizer with high singlet oxygen generation ability in visible light (400–700 nm). Confocal microscopy using the emissive complex **1** showed significant mitochondrial localization of the complex. Cell death via apoptotic pathway was observed from the Annexin-V-FITC/PI assay. The formation of Pt-DNA adducts was evidenced from the binding experiments of the complexes **1** and **2** with 9-ethylguanine as a model nucleobase from  $^1\text{H}$  NMR and mass spectral studies.



## INTRODUCTION

Cisplatin and its analogues, specifically, carboplatin and oxaliplatin, are well-known chemotherapeutic drugs, while nedaplatin, lobaplatin, and heptaplatin are subsequently developed as potential chemotherapeutic agents.<sup>1–5</sup> These drugs act as transcription inhibitors with the formation of cross-links with nuclear DNA through covalent bond formation involving platinum(II) and the N<sup>7</sup> atoms of guanine residues resulting in apoptotic cell death. Kinetics of dissociation of the anionic ligand and the physicochemical properties of the Pt-DNA adducts play major roles in the overall efficacy of the drug.<sup>6–9</sup> These bifunctional drugs are associated with some undesirable side effects that include poor tumor selectivity, intrinsic and/or acquired resistance, besides reduced activity due to nuclear excision repair (NER) mechanism being operative for the nuclear DNA. To overcome these major deficiencies, novel six-coordinate platinum(IV) complexes with two labile axial ligands are developed as prodrugs that get converted to the active platinum(II) species by photochemical or chemical means using light as an activator or cellular glutathione acting as a reducing agent for platinum(IV).<sup>10–13</sup>

A new approach to overcome these shortcomings leads to the recent development of the chemistry of cationic monofunctional platinum(II) complexes.<sup>12–18</sup> Such complexes like pyriplatin and its analogues display markedly different anticancer activity because of their altered cellular response when compared to the classical bifunctional platinum-based drugs, specifically, cisplatin (Figure 1). Monofunctional platinum(II) complexes, specifically,  $[(\text{dien})PtCl]^+$  and  $[(\text{NH}_3)_3PtCl]^+$ , are reported to show inactivity toward cancer cells, while phenanthriplatin and pyriplatin, reported by Lippard and co-workers, have shown varied anticancer activity requiring further studies on these monofunctional platinum(II) complexes.<sup>1,19</sup> The observed less potency than cisplatin and its analogues under chemotherapeutic conditions has led to the pertinent question about how the efficacy of the monofunctional anticancer agents can be enhanced. An effective way to address this problem is to design complexes that show dual activity by choosing a suitable photosensitizer (PS) appended to the ligand bound to platinum(II). While the PS can show

Received: May 25, 2017

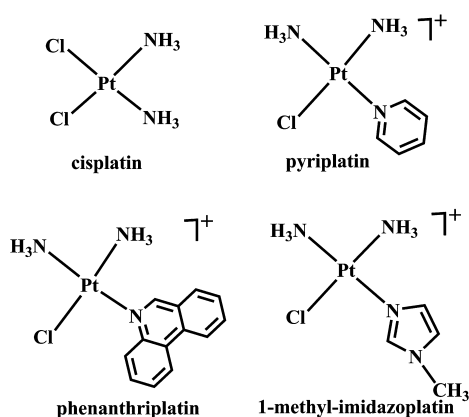


Figure 1. Bifunctional cisplatin and its monofunctional analogues.

photodynamic therapy (PDT) effect, the complex bearing a labile anionic ligand, which is generally a chloride in majority of these compounds, can act as a DNA cross-linking agent.<sup>20–28</sup> Such a complex can then be used as a transcription inhibitor on labilizing the anionic ligand, while the appended photosensitizer can generate reactive oxygen species (ROS) in a similar way as is known in PDT of macrocyclic porphyrinic dyes, specifically, Photofrin and its analogues.<sup>29–37</sup>

There are few reports of platinum(II) conjugates having appended macrocyclic PDT-based photosensitizers. Guo and co-workers first reported a “molecular combo” in which silicon(IV) phthalocyanine moiety, as a red-light PDT agent, is attached to the pyriplatin moiety acting as a transcription inhibitor.<sup>38</sup> Doherty and co-workers have reported photodynamic cellular damage of cancer cells by a platinum(II) complex of a cyclometalating ligand.<sup>39</sup> Besides the porphyrin dyes, photosensitizers based on non-macrocyclic dyes could be used toward designing conjugates to achieve the combined effect of PDT and a DNA transcription inhibitor. Recently, fluorescent 4,4-difluoro-4-bora-3a,4a-diaza-*s*-indacene (BODIPY)-platinum conjugates are reported for cellular imaging and as theranostic agents, predominantly localizing into the mitochondria (mt) of the cells.<sup>40–42</sup> Such complexes are of significance, as the NER mechanism is absent for mtDNA. A rational approach could lead to the development of new generation of dual action anticancer agents. The present work stems from our efforts to design monofunctional imidazoplatin analogues with appended BODIPY moiety for cellular imaging and its diiodo derivative for generating singlet oxygen ( $^1\text{O}_2$ ) via type-II pathway on photoactivation by visible light (400–700 nm) to damage the cancer cells. Herein, we report three monofunctional imidazoplatin complexes of formulation  $\text{cis-}[\text{Pt}(\text{NH}_3)_2(\text{L})\text{Cl}](\text{NO}_3)$  (1–3), where L is imidazole conjugated to BODIPY ( $\text{L}^1$  in 1) and the diiodo-BODIPY ( $\text{L}^2$  in 2) and 1-methylimidazole (1-MeIm in 3) as a control (Figure 2). The complexes were synthesized and characterized, and their cellular activity in dark and light was studied. Complex 3 was used for structural characterization by X-ray crystallography. Significant results of this work are the remarkable singlet oxygen-induced PDT effect of the nonfluorescent complex 2, named as “Imidazoplatin-B”, giving  $\text{IC}_{50}$  value in nanomolar concentration, while cellular imaging done using fluorescent complex 1 showed its significant mitochondrial localization in HaCaT and MCF-7 cells. In addition, both the BODIPY-appended imidazoplatin complexes, specifically,  $\text{cis-}[\text{Pt}$

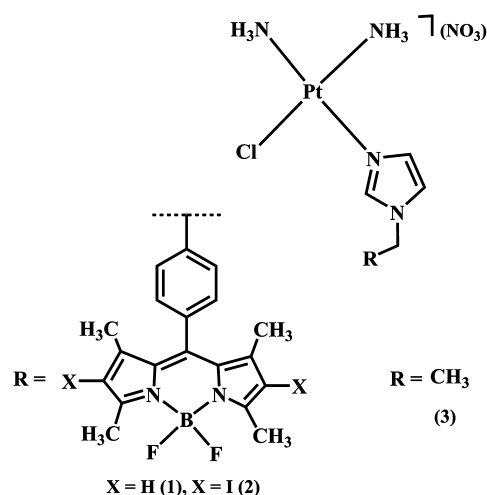


Figure 2. Chemical structures of the platinum(II) complexes 1–3 and the ligands used.

$(\text{NH}_3)_2(\text{L}^1)\text{Cl}](\text{NO}_3)$  (1) and  $\text{cis-}[\text{Pt}(\text{NH}_3)_2(\text{L}^2)\text{Cl}](\text{NO}_3)$  (2), showed their ability for DNA cross-link formation.

## EXPERIMENTAL SECTION

**Materials and Methods.** Cisplatin was purchased from Arora Matthey, India. Mito-Tracker Deep Red FM (MTR) and ER-Tracker Deep Red (ERTR) were purchased from Invitrogen (USA). All other chemicals and reagents were obtained from S. D. Fine Chemicals (India) and Sigma-Aldrich (USA). Tetrabutylammonium perchlorate (TBAP) was prepared by treating tetrabutylammonium bromide with perchloric acid. Complex 3 was prepared by following a literature report.<sup>14</sup> All NMR spectra were recorded using a Bruker Avance NMR spectrometer. Mass spectral data were acquired with an Agilent 6538 Ultra High Definition Accurate Mass-Q-TOF (LC-HRMS) instrument. Elemental analysis was performed with a Thermo Finnigan Flash EA 1112 CHNS analyzer. IR, UV–visible, and emission spectra were recorded with Bruker Alpha and PerkinElmer Spectrum 750 spectrophotometers and HORIBA Jobin Yvon IBH TCSPC fluorimeter (fitted with FluoroHub software analysis). Cyclic voltammetric studies were performed with an EG&G PAR model 253 VersaStat potentiostat/galvanostat. A three-electrode setup was used (glassy carbon electrode as the working electrode, a platinum wire as the auxiliary electrode, and saturated calomel electrode (SCE) as the reference). Ferrocene was used as a standard ( $E_f = 0.47$  V vs SCE at  $50$   $\text{mV s}^{-1}$ ). TBAP (0.1 M) was used as a supporting electrolyte. All experiments requiring light exposure were performed with a broad-band white light using Luzchem Photoreactor (model LZC-1, Ontario, Canada) fitted with eight fluorescent Sylvania white tubes ( $\lambda = 400$ – $700$  nm) and standard protocols. Cytotoxic data were obtained with a TECAN microplate reader and fitted using GraphPad Prism 7 software. Flow cytometric experiments were performed using fluorescence-activated cell sorting (FACS) Verse instrument (BD Biosciences) fitted with a MoFlo XDP cell sorter and analyzer with three lasers ( $\lambda = 488, 365,$  and  $640$  nm) and 10-color parameters. Confocal microscopy images were acquired from Leica microscope (TCS, SP5) with an oil immersion lens with magnification of 63 $\times$ . Images were processed by using LAS AF Lite software.

**Synthesis.** The synthetic steps employed for the preparation of the ligands and the complexes are given in Scheme S1 (see Supporting Information). A brief writeup with the characterization data is given below.

**Ligand L<sup>1</sup>.** A mixture of 4,4-difluoro-8-(4-chloromethylphenyl)-1,3,5,7-tetramethyl-4-bora-3a,4a-diaza-*s*-indacene<sup>43</sup> (750 mg, 2.02 mmol, 1.0 equiv),  $\text{K}_2\text{CO}_3$  (555 mg, 4.02 mmol, 2.0 equiv), and KI (667 mg, 4.02 mmol, 2.0 equiv) in aqueous acetonitrile (1:2 v/v, 30 mL) was purged with nitrogen for 30 min. Imidazole (123 mg, 1.80 mmol, 0.9 equiv) was added, and the solution was heated for reflux at

95 °C for 16 h under nitrogen atmosphere. After it cooled to room temperature and was diluted with dichloromethane, it was washed with water and brine. The organic phase was collected, dried over sodium sulfate, filtered, and concentrated under reduced pressure by rotary evaporator. The crude product thus obtained was purified by silica gel column chromatography by eluting with chloroform–ethyl acetate (9:1 v/v with 1% methanol) to yield the desired greenish-orange product. Yield = 390 mg (0.96 mmol, 48%). Anal. Calcd for  $C_{23}H_{23}BF_2N_4$  ( $M_w$ : 404.19): C, 68.33; H, 5.73; N, 13.86. Found: C, 68.10; H, 5.87; N, 13.56%. Electrospray ionization mass spectrometry (ESI-MS) ( $m/z$ ) in MeOH: 405.20  $[M + H]^+$ .  $^1H$  NMR (400 MHz, deuterated dimethyl sulfoxide (DMSO- $d_6$ )): 7.76 (s, 1 H), 7.42–7.35 (m, 4 H), 7.18 (s, 1 H), 6.94 (s, 1 H), 6.16 (s, 2 H), 5.31 (s, 2 H), 2.44 (s, 6 H), 1.31 (s, 6 H) (s, singlet; m, multiplet).  $^{13}C$  NMR (100 MHz, DMSO- $d_6$ ): 155.40, 143.14, 142.02, 139.18, 137.88, 133.88, 131.13, 128.90, 128.76, 121.69, 120.09, 49.69, 29.42 14.66, 14.45 ppm. IR data ( $cm^{-1}$ ): 2920 (sh), 2850 (s), 1536 (sh), 1505 (sh), 1300 (sh), 1190 (w), 1150 (s), 960 (sh), 810 (s), 720 (sh) (w, weak; s, strong; sh, shoulder). UV–visible (1% DMSO/Dulbecco's Modified Eagle's Medium (DMEM) at pH 7.2) [ $\lambda_{max}$  nm ( $\epsilon$ ,  $M^{-1} cm^{-1}$ ): 500 (33 100). Emission data (1% DMSO/DMEM at pH 7.2):  $\lambda_{em}$  ( $\lambda_{ex}$   $\Phi_f$ ) = 505 nm (490 nm, 0.17).

**Ligand L<sup>2</sup>.** Ligand L<sup>1</sup> (202 mg, 0.5 mmol) was dissolved in dry dichloromethane (30 mL), excess of *N*-iodo succinimide (675 mg, 3 mmol, 6 equiv) was added, and the mixture was stirred for 14 h under nitrogen atmosphere. The red solution was diluted with dichloromethane and washed with water. The organic phase was dried over sodium sulfate, filtered, and concentrated under reduced pressure by rotary evaporator. The crude product was purified by silica gel column chromatography using chloroform/ethyl acetate (9:1 v/v with 1% methanol) as eluent to isolate the product as pink-red solid. Yield = 210 mg (0.32 mmol, 64%). Anal. Calcd for  $C_{23}H_{21}BF_2I_2N_4$  ( $M_w$ : 655.99): C, 42.11; H, 3.23; N, 8.54. Found: C, 42.07; H, 3.21; N, 8.43%. ESI-MS  $m/z$  in MeOH: 656.98  $[M + H]^+$ .  $^1H$  NMR (DMSO- $d_6$ , 400 MHz): 8.44 (s, 1 H), 7.95 (s, 2 H), 7.45–7.39 (m, 4 H), 7.24 (s, 1 H), 7.01 (s, 1 H), 5.35 (s, 2 H), 2.56 (s, 6 H), 1.31 (s, 6 H).  $^{13}C$  NMR (100 MHz, DMSO- $d_6$ ): 163.22, 157.03, 145.77, 142.27, 139.23, 138.22, 135.19, 134.70, 131.70, 129.50 129.14, 128.76, 120.74, 87.87, 50.28, 36.69, 31.68, 30.43, 17.51, 16.66 ppm. IR data ( $cm^{-1}$ ): 2920 (sh), 2855 (s), 1695 (sh), 1525 (sh), 1340 (s), 1175 (s), 990 (s), 800 (br) (br, broad). UV–visible (1% DMSO/DMEM at pH 7.2) [ $\lambda_{max}$  nm ( $\epsilon$ ,  $M^{-1} cm^{-1}$ ): 540 (15 700), 515 (13 500).

**cis-[Pt(NH<sub>3</sub>)<sub>2</sub>(L)Cl](NO<sub>3</sub>) (1, 2).** The monofunctional platinum(II) complexes were prepared by modifying the literature procedure.<sup>14,40</sup> To a solution of cisplatin (0.15 g, 5 mmol) in 5 mL of *N,N*-dimethylformamide (DMF) was added AgNO<sub>3</sub> (0.89 g, 1 equiv), and the reaction mixture was stirred under protection from light at room temperature for 24 h. AgCl precipitate formed was removed by filtration. To the solution was added the ligand (L<sup>1</sup> and L<sup>2</sup>, 0.9 equiv), and the reaction mixture was stirred for 24 h at 28 °C. The solvent was evaporated under reduced pressure, and the residue was dissolved in 30 mL of MeOH. Unreacted yellow cisplatin was removed by filtration. The filtrate was stirred vigorously, and diethyl ether (60 mL) was added to precipitate the desired compound as solid. The product was isolated, washed twice with 50 mL of diethyl ether, vacuum-dried, and kept in dark.

**cis-[Pt(NH<sub>3</sub>)<sub>2</sub>(L<sup>1</sup>)Cl](NO<sub>3</sub>) (1).** Greenish-black solid. Yield: 72%. Anal. Calcd for  $C_{23}H_{29}BClF_2N_7O_3Pt$  ( $M_w$ : 730.17): C, 37.80; H, 4.00; N, 13.42. Found: C, 37.61; H, 3.83; N, 13.36%. ESI-MS ( $m/z$ ): Calcd  $[M-NO_3]^+$ , 668.19; Found: 668.18.  $^1H$  NMR (400 MHz, DMSO- $d_6$ ):  $\delta$  8.76 (s, 1 H), 7.86 (s, 1 H), 7.47–7.40 (m, 4 H), 7.09 (s, 1 H), 6.17 (s, 2 H), 5.59 (s, 2 H), 4.18 (s, 3 H), 3.94 (s, 3 H), 2.44 (s, 6 H), 1.32 (s, 6 H).  $^{13}C$  NMR (100 MHz, DMSO- $d_6$ ):  $\delta$  155.03, 143.77, 142.27, 139.96, 137.23, 133.03, 131.19, 128.70, 128.50, 128.17, 121.76, 120.74, 80.42, 49.66, 29.42, 14.69, 14.45. IR data ( $cm^{-1}$ ): 3300 (br), 3130 (br), 1540 (s), 1500 (s), 1300 (br), 1190 (s), 1150 (s), 975 (br). UV–visible (1% DMSO/DMEM at pH 7.2):  $\lambda_{max}$  nm ( $\epsilon$ ,  $M^{-1} cm^{-1}$ ) = 530 (18 000), 500 (27 000). Emission (1% DMSO/DMEM at pH 7.2):  $\lambda_{em}$  ( $\lambda_{ex}$   $\Phi_f$ ) = 510 nm (490 nm, 0.09).

**cis-[Pt(NH<sub>3</sub>)<sub>2</sub>(L<sup>2</sup>)Cl](NO<sub>3</sub>) (2).** Red solid. Yield: 76%. Anal. Calcd for  $C_{23}H_{27}BClF_2I_2N_7O_3Pt$  ( $M_w$ : 981.96): C, 28.11; H, 2.77; N, 9.98. Found: C, 28.10; H, 2.74; N, 9.99%. ESI-MS ( $m/z$ ): Calcd  $[M-NO_3]^+$ , 919.98; Found, 919.98.  $^1H$  NMR (400 MHz, DMSO- $d_6$ ):  $\delta$  7.80 (s, 1 H), 7.46–7.40 (m, 4 H), 7.11 (s, 2 H), 5.55 (s, 2 H), 4.14 (s, 3 H), 3.95 (s, 3 H), 2.40 (s, 6 H), 1.33 (s, 6 H).  $^{13}C$  NMR (100 MHz, DMSO- $d_6$ ):  $\delta$  163.76, 157.42, 145.77, 142.27, 139.96, 138.23, 135.03, 134.65, 131.66, 129.31, 129.14, 128.76, 120.74, 87.93, 50.28, 36.81, 32.45, 30.43, 17.61, 16.66. IR data ( $cm^{-1}$ ): 3300 (br), 3190 (br), 1610 (br), 1525 (sh), 1340 (s), 1300 (w), 1170 (sh), 1000 (sh). UV–visible (1% DMSO/DMEM at pH 7.2):  $\lambda_{max}$  nm ( $\epsilon$ ,  $M^{-1} cm^{-1}$ ) = 540 (14 300), 510 (19 000).

**X-ray Crystallographic Procedure.** The crystal structures of complex 3 and ligand L<sup>1</sup> were obtained by single-crystal X-ray diffraction method. The colorless rectangular block crystals of complex 3 were obtained from aqueous methanol on slow evaporation, while L<sup>1</sup> as red rectangular blocks were crystallized from dimethyl sulfoxide solution on slow evaporation. Both the crystals were mounted on loops with mineral oil. All intensity and geometric data were collected by an automated Bruker SMART APEX CCD diffractometer equipped with a fine focus 1.75 kW sealed-tube Mo  $K\alpha$  X-ray source ( $\lambda = 0.71073 \text{ \AA}$ ) with increasing  $\omega$  (width of 0.3° per frame) at a scan speed of 5 s frame<sup>-1</sup>. Intensity data were collected using the  $\omega$ -2 $\theta$  scan mode and then corrected for Lorentz-polarization and absorption effects.<sup>44</sup> The structures were solved and refined using the WinGX suite of programs (version 1.63.04a) by the SHELXL-2013 method.<sup>45</sup> The non-hydrogen atoms were refined with anisotropic displacement coefficients, and their coordinates were permitted to ride on their respective carbon atoms. Atomic positions for all the atoms, anisotropic thermal parameters for all the non-hydrogen atoms, and isotropic thermal parameters for all the hydrogen atoms were included in the final refinement. The perspective views were obtained using ORTEP.<sup>46</sup> Selected crystallographic parameters, bond distances, and angles data are given in Table 2 and Table S1 (see Supporting Information). The CCDC deposition numbers are 1524705 and 1524706.

**Cellular and DNA Binding Experiments.** The cytotoxicity studies of the platinum complexes 1 and 2 and their ligands L<sup>1</sup> and L<sup>2</sup> were made by 3-(4,5-dimethylthiazol-2-yl)-2,5-diphenyltetrazolium bromide (MTT) assay using HaCaT (human keratinocyte) and MCF-7 (human breast cancer) cells. Cells were incubated with various concentrations of the complexes from 0.14 to 10  $\mu M$  in 1% DMSO/DMEM for 4 h in the dark. One set of the cells was exposed to visible light for 1 h ( $\lambda = 400$ –700 nm, light dose = 10 J cm<sup>-2</sup>), while the other set was kept in the dark for 1 h using standard protocols.<sup>47</sup> The samples were kept for another 19 h incubation in dark thus making the total incubation period for the MTT assay as 24 h. Data were obtained from three independent sets of experiments done in triplicate for each concentration. The intracellular localization of complex 1 was investigated by confocal microscopy. HaCaT cells were incubated with the complex (10  $\mu M$  in 1% DMSO/DMEM) in the dark for 4 h. Cells were stained with 4',6-diamidino-2-phenylindole (DAPI; 1 mg mL<sup>-1</sup>) for 5 min. Live cells were stained with MTR (100 nM) and ERTR (100 nM). Images were captured in a Leica microscope (TCS, SP5) with an oil immersion lens and magnification of 63 $\times$ . Multiple images were recorded, and experiments were done in duplicate. The photoinduced generation of reactive oxygen species (ROS) by the complexes in 1% DMSO/DMEM in HaCaT was quantified by using the 2,7-dichlorofluorescein diacetate (DCFDA) assay. Cells were incubated with 1 (5  $\mu M$ ) and 2 (2.5  $\mu M$ ) for 4 h in dark. One of the plates was irradiated ( $\lambda = 400$ –700 nm, light dose = 10 J cm<sup>-2</sup>) for 1 h in PBS buffer, whereas the other was kept in the dark. Annexin-V/FITC/PI assay was done for 1 (5  $\mu M$ ) and 2 (2.5  $\mu M$ ) in 1% DMSO/DMEM. Approximately 3  $\times 10^5$  HaCaT cells were seeded in six-well plates and cultured for 24 h. The cells were incubated with the complex for 4 h in the dark and then exposed to light (1 h,  $\lambda = 400$ –700 nm, light dose = 10 J cm<sup>-2</sup>) in phenol red free media or kept in dark. Cells were then kept for another 14 h in DMEM/10% fetal bovine serum (FBS) buffer in the dark, after which the medium was discarded, and the cells were trypsinized and resuspended in the

Table 1. Selected Physicochemical Data for Complexes 1 and 2 along with Ligands L<sup>1</sup> and L<sup>2</sup>

complex	$\Lambda_m^a/S\ m^2\ M^{-1}$	$\lambda_{max}^b/nm\ (\times 10^{-4}\ \epsilon\ [M^{-1}\ cm^{-1}])$	$\lambda_{em}^c/nm\ (\Phi_f)$	$E_{pc}^d/V$	$K_b^e/M^{-1}$	$\Delta T_m^f/^\circ C$
1	77	530 (1.8), 500 (2.7)	510 (0.09)	-0.63	$1.2 (\pm 0.3) \times 10^4$	3
2	80	540 (1.4), 510 (1.9)		-0.87	$1.5 (\pm 0.1) \times 10^4$	2
L <sup>1</sup>		500 (3.3)	505 (0.17)	-0.56		
L <sup>2</sup>		540 (1.5), 515 (1.3)		-0.81		

<sup>a</sup>Molar conductivity in DMF. <sup>b</sup>In 1% DMSO/DMEM mixture. <sup>c</sup>In 1% DMSO/DMEM solution. <sup>d</sup>Cathodic peak potential in DMF-0.1 M TBAP. The potentials are versus SCE. Scan rate = 50 mV s<sup>-1</sup>. <sup>e</sup>Intrinsic equilibrium ct-DNA binding constant,  $K_b$  from UV-visible absorption spectral experiments. <sup>f</sup>Change in ct-DNA melting temperature.

binding buffer (300 mL, 1X). Annexin-V/FITC (0.5 mL) and propidium iodide (PI; 1 mL) were added to the cell suspensions and incubated for 5 min. Readings were taken with the FACS instrument. The effect of 1 and 2 on the cell cycle progress was analyzed by cell-cycle analysis in which  $\sim 1 \times 10^6$  HaCaT cells were cultured in six-well tissue culture plates in DMEM/FBS (10%) for 24 h. The 1% DMSO/DMEM solutions of 1 (5  $\mu$ M) and 2 (2.5  $\mu$ M) were added to the cells and incubated for 4 h in the dark. After that, one of the complex-treated plates was subjected to irradiation in phenol red free media ( $\lambda = 400$ –700 nm, light dose = 10 J cm<sup>-2</sup>), whereas the identical other set was kept in the dark. After the irradiation, postincubation was done for 19 h in the dark. Cells were then processed and analyzed with a FACS Verse machine (BD Biosciences) at the FL2 channel ( $\lambda = 595$  nm). The populations of cells were obtained from histograms generated by the Cell Quest Pro software (BD Biosciences). Experiments were performed in duplicate, along with untreated controls. Calf thymus (ct) DNA (200  $\mu$ M) was treated with the complexes 1 and 2 (25  $\mu$ M) in 1% DMF-Tris buffer (pH = 7.2), and a detailed writeup on the DNA melting and viscosity experiments is provided as Supporting Information.

## RESULTS AND DISCUSSION

**Synthesis and General Aspects.** The imidazoplatin derivatives [Pt(NH<sub>3</sub>)<sub>2</sub>(L)Cl](NO<sub>3</sub>), where L is L<sup>1</sup> with a BODIPY moiety in 1 and L<sup>2</sup> with a diiodo BODIPY moiety in 2 and 1-methylimidazole in 3, were prepared by following a general synthetic procedure in which cisplatin was first treated with silver nitrate followed by the addition of the corresponding ligand in DMF (Figure 2).<sup>14,40</sup> The ligands and their platinum(II) complexes were characterized from the spectral and analytical data. Selected physicochemical data are given in Table 1. The ESI mass spectra of the complexes 1 and 2 in MeOH showed primarily the [M-(NO<sub>3</sub>)]<sup>+</sup> peak in accordance with the calculated  $m/z$  values. The isotopic distribution pattern indicated the presence of platinum and unipositive charge of the complexes (Figures S1–S4, Supporting Information). The diamagnetic platinum(II) complexes displayed <sup>1</sup>H NMR spectra with characteristic singlet peak in the range of 5.30–6.30 ppm assignable to the hydrogen atom of the methylene protons.<sup>42</sup> The peaks of the BODIPY unit at  $\delta = 6.16$  ppm are for  $\gamma$ -proton; the aromatic hydrogen atoms were in the range of 7.35–7.45 ppm, and the methyl groups were at  $\delta = 2.44$  and 1.31 ppm (Figures S5–S8, Supporting Information). The peaks for protons corresponding to the imidazole moiety in L<sup>1</sup> and L<sup>2</sup> are within 6.78–7.94 ppm. The absence of  $\gamma$ -proton signals in L<sup>2</sup> at  $\delta = 6.16$  is due to diiodination of L<sup>1</sup>. The <sup>13</sup>C NMR spectra for these ligands and their metal complexes showed the presence of aliphatic CH<sub>2</sub> (methylene moiety) carbon, giving signals within 50–55 ppm (Figures S9–S12, Supporting Information). The aromatic carbon atoms appeared in the range of 110–170 ppm, and the aliphatic methyl carbons were within 14–35 ppm. Two new peaks at 30 and 87 ppm in <sup>13</sup>C NMR were assigned to the iodinated carbon atoms. The <sup>1</sup>H and <sup>13</sup>C NMR spectra of the

complexes showed peaks that are similar to those observed for the free ligands. Some additional peaks within the range of 3.94–4.40 ppm observed in the <sup>1</sup>H NMR spectra were assigned for protons of two ammine ligands. The <sup>11</sup>B NMR spectra gave a characteristic triplet signal at 0.82–0.16 ppm, with a coupling constant of 33 Hz resulting from coupling of two equivalent fluorine nuclei. The upfield shift in the <sup>11</sup>B NMR of ligands from L<sup>1</sup> to L<sup>2</sup> by 0.15 ppm indicates the effect of diiodination of L<sup>1</sup> on the boron atom (Figures S13 and S14, Supporting Information).<sup>48</sup> The <sup>19</sup>F NMR spectra showed a distinct influence of the imidazole moieties. It is known that small changes on the symmetry of the molecule, even at large distance to the <sup>19</sup>F core, significantly alter the NMR spectra of the BODIPY moieties.<sup>49</sup> The symmetrical BODIPY derivatives L<sup>1</sup> and L<sup>2</sup> showed a single quartet and quintet spectra (Figures S15 and S16, Supporting Information). IR spectra of the free ligands showed two intense peaks within 1610–1600 and 1560–1510 cm<sup>-1</sup> due to respective C=N and conjugated C=C of imidazole ring-stretching frequencies.<sup>50</sup> The metal-bound NH<sub>3</sub> of cisplatin analogues showed sharp characteristic peaks near 3500–3300 cm<sup>-1</sup> indicating their presence in the complexes (Figures S17–S20, Supporting Information).

The complexes are 1:1 electrolytic giving molar conductivity values of  $\sim 78$  S m<sup>2</sup> M<sup>-1</sup> in DMF at 25  $^\circ$ C. The purity of the complexes was ascertained from the elemental analysis and NMR spectral data. The absorption spectra of the complexes were recorded in 1% DMSO/DMEM, pH = 7.2. Complexes 1 and 2 displayed strong absorption band near 500 and 510 nm, which is assignable to the electronic transition involving the BODIPY unit (Figure S21, Supporting Information).<sup>51</sup> In addition, the BODIPY complexes showed additional band at 530 and 540 nm. The BODIPY moiety in complex 1 showed an intense emission band at 510 nm ( $\lambda_{ex} = 470$  nm) making it suitable for cellular imaging study with an  $\Phi_F$  value of 0.09 (Figure 3). The free ligand L<sup>1</sup> gave an emission spectrum with higher  $\Phi_F$  value ( $\Phi_F$ : 0.17) than the complex. Complex 2 and ligand L<sup>2</sup> showed no apparent emission band. The presence of

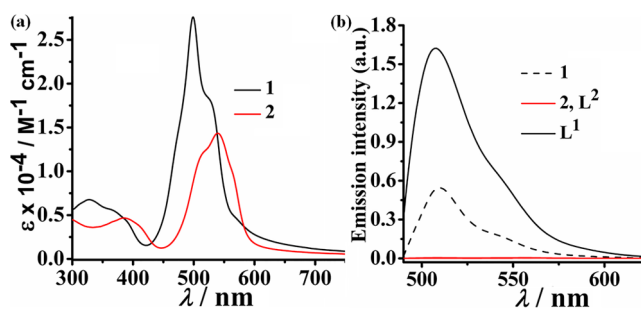
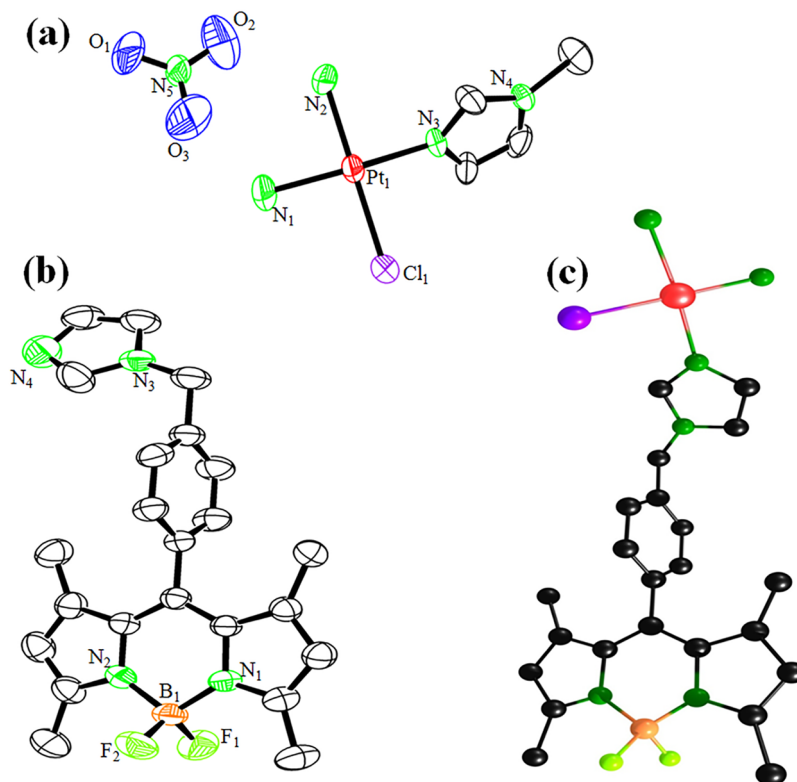


Figure 3. (a) Absorption spectra of the complexes 1 and 2 and (b) emission spectra ( $\lambda_{ex} = 490$  nm) of the ligands L<sup>1</sup> and L<sup>2</sup> and the complexes 1 and 2 in 1% DMSO-DMEM solution (pH = 7.2).



**Figure 4.** An ORTEP view of the cationic complex of **3** (a) and ligand **L**<sup>1</sup> (b) showing thermal ellipsoids at a 50% probability level. (c) The energy-minimized structure of complex **1** using B3LYP/LANL2DZ level of theory. Color codes: Pt red, F parrot green, Cl purple, N green, and C black. Hydrogen atoms are omitted for clarity.

two heavy iodine atoms in **L**<sup>2</sup> and **2** makes efficient intersystem crossing (ISC) thus resulting in diminished fluorescence intensity by facilitating the type-II process. The redox activity of the complexes was studied by cyclic voltammetry in DMF–0.1 M tetrabutylammonium perchlorate (TBAP). The cyclic voltammogram of the BODIPY ligand **L**<sup>1</sup> has a cathodic peak near –0.6 V (vs SCE). The reduction peak was observed at –0.8 V in **L**<sup>2</sup>. The responses were observed near –0.6 V for **1** and –0.9 V for **2** involving the BODIPY core (Figures S22 and S23, Supporting Information). The complexes were soluble in common organic solvents other than hydrocarbons. They were fairly stable in both solid and solution phases. The stability of the complexes was studied in the dark and light (400–700 nm) in the presence of cellular analytes by UV–visible measurements up to 48 h (Figure S24, Supporting Information).

**Crystallography and Theoretical Study.** Complex **3** and ligand **L**<sup>1</sup> were structurally characterized by single-crystal X-ray crystallography (Figure 4, Table 2, and Figures S25–S27, Supporting Information). Complex **3** crystallized in the space group *Pn*2<sub>1</sub>*a* of the orthorhombic crystal system having nitrate as the counteranion (Figure 4a). The complex in a square planar geometry has the platinum(II) coordinated to three N-donor atoms, specifically, two cis-oriented ammine groups and an imidazole moiety with one chloride ligand bound to the fourth coordination site. The Pt–N bond distances in **3** are 2.019(15), 2.045(15), and 2.027(14) Å for the two ammines and imidazole, respectively. The Pt–Cl distance is 2.293(5) Å, and the NH<sub>3</sub>–Pt–NH<sub>3</sub> angle is 87.0(6)°. The Pt–Cl bonds in cisplatin of 2.3088(19) and 2.313(2) Å are marginally longer than in **3**.<sup>52</sup> The unit-cell packing diagram of **3** showed the hydrogen bonding interaction between the hydrogen atoms of the ammine with the counteranion and the chloride ligand.

**Table 2.** Selected Crystallographic Data of Complex *cis*-[Pt(NH<sub>3</sub>)<sub>2</sub>(1-MeIm)Cl](NO<sub>3</sub>) (**3**) and Ligand **L**<sup>1</sup>

	complex <b>3</b>	<b>L</b> <sup>1</sup>
empirical formula	C <sub>4</sub> H <sub>12</sub> ClN <sub>3</sub> O <sub>3</sub> Pt	C <sub>23</sub> H <sub>23</sub> BF <sub>2</sub> N <sub>4</sub>
Fw/g M <sup>-1</sup>	408.72	404.26
crystal system	orthorhombic	monoclinic
space group	<i>Pn</i> 2 <sub>1</sub> <i>a</i>	<i>P</i> 2 <sub>1</sub> / <i>n</i>
<i>a</i> /Å	11.2658(5)	16.4581(14)
<i>b</i> /Å	4.2853(2)	6.8134(6)
<i>c</i> /Å	22.1688(10)	18.9014(15)
$\alpha$ /deg	90	90
$\beta$ /deg	90	107.176(2)
$\gamma$ /deg	90	90
<i>V</i> /Å <sup>3</sup>	1070.25(8)	2025.0(3)
<i>Z</i>	4	4
<i>T</i> , K	298	298
$\rho_{\text{calc}}$ /Mg m <sup>-3</sup>	2.537	1.326
$\lambda$ /Å (Mo–K $\alpha$ )	0.710 73 Å	0.710 73 Å
data/restraints/param	2480/1/127	6048/0/271
<i>F</i> (000)	660.0	848.0
GOF	1.033	1.011
<i>R</i> ( <i>F</i> <sub>o</sub> ), <sup>a</sup> <i>I</i> > 2 $\sigma$ ( <i>I</i> ) [ <i>wR</i> ( <i>F</i> <sub>o</sub> ) <sup>b</sup> ]	0.0420 [0.1016]	0.0786 [0.1835]
<i>R</i> (all data) [ <i>wR</i> (all data)]	0.0621 [0.1097]	0.2134 [0.2373]
largest diff peak, hole (e Å <sup>-3</sup> )	0.947, –0.697	0.377, –0.289
$w = 1/[(\sigma F_o)^2 + (AP)^2 + (BP)]$	A = 0.0513 B = 11.6829	A = 0.1064 B = 0.8163

<sup>a</sup>*R* =  $\sum |F_o| - |F_c| / \sum |F_o|$ . <sup>b</sup>*wR* =  $\{ \sum [w(F_o^2 - F_c^2)^2] / \sum [w(F_o^2)] \}^{1/2}$ , where  $P = (F_o^2 + 2F_c^2) / 3$ .

Ligand **L**<sup>1</sup> crystallized in the monoclinic space group *P*2<sub>1</sub>/*n*. The bond lengths of B(1)–F(1) and B(1)–F(2) are 1.389(3)

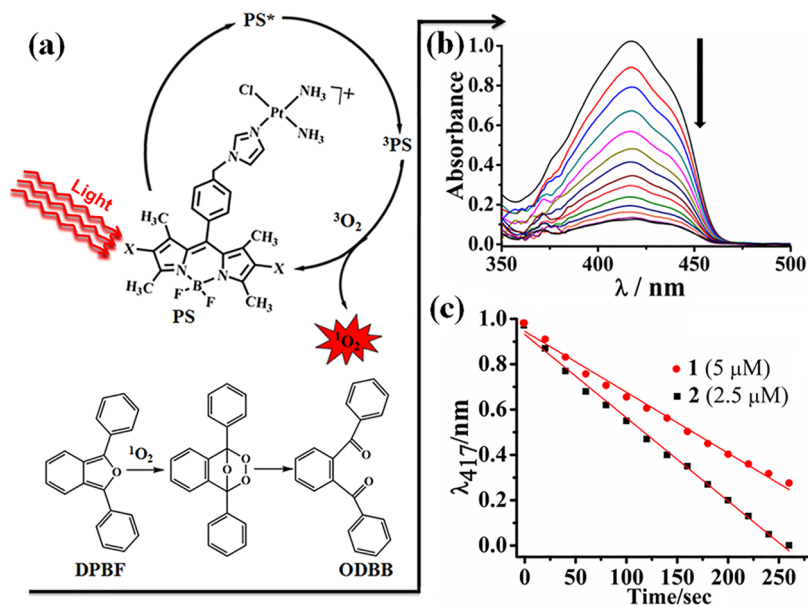


**Figure 5.** (a) Schematic diagram of  $^1\text{O}_2$  generation and quenching of DPBF [PS: ground singlet state, PS\*: excited singlet states or higher states,  $^3\text{PS}$ : triplet state,  $^3\text{O}_2$  and  $^1\text{O}_2$ : oxygen molecule in its triplet ground state and in the singlet excited state]. (b) Spectral changes of DPBF treated with **2** in DMF. (c) Oxidation of DPBF to ODBB (*o*-dibenzoylbenzene) by  $^1\text{O}_2$  from photoexposure of **1** ( $5\ \mu\text{M}$ ) and **2** ( $2.5\ \mu\text{M}$ ) in DMF.

and  $1.377(3)\ \text{\AA}$ , respectively (Figure 4b). The N(1)–B(1) and N(3)–B(1) bonds are of  $1.540(4)$  and  $1.539(4)\ \text{\AA}$ . The F(1)–B(1)–F(2) and N(1)–B(1)–N(2) angles are  $109.8(2)^\circ$  and  $107.2(2)^\circ$ . The structural data of complex **3** and  $L^1$  were used to generate the energy-optimized structures of the complexes **1** and **2** by employing quantum calculations with B3LYP/LANL2DZ level of theory for all atoms (Figure 4c, Table S2, and Figures S28 and S29, Supporting Information).<sup>53–55</sup> The frontier orbitals were mapped on the atoms from the distribution of the electronic charge density. The highest occupied molecular orbital (HOMO) for the complexes **1** and **2** is found to be localized on the platinum-imidazole core, while the lowest unoccupied molecular orbital (LUMO) is primarily localized on the BODIPY moiety.

**Singlet Oxygen Generation.** An important aspect of photodynamic therapy (PDT) of cancer is the involvement of singlet oxygen ( $^1\text{O}_2$ ) generated via type-II energy transfer pathway as the ROS for which there is no apparent defense mechanism available in the cellular system.<sup>31</sup> The objective of appending a diiodo-BODIPY unit on the imidazole base is to photogenerate singlet oxygen species. This was studied from the 1,3-diphenylisobenzofuran (DPBF) experiments.<sup>56</sup> DPBF being photostable in DMF, the singlet oxygen quenching experiments were performed in DMF solutions of the complexes (Figure 5a). Complex **1** ( $5\ \mu\text{M}$ ), the diiodo-BODIPY complex **2** ( $2.5\ \mu\text{M}$ ), and free ligands  $L^1$  ( $5\ \mu\text{M}$ ) and  $L^2$  ( $2.5\ \mu\text{M}$ ) were treated with DPBF ( $50\ \mu\text{M}$ ) in DMF. The absorption spectra were recorded at an excitation wavelength of  $417\ \text{nm}$  (Figure 5b, Figures S30 and S31, Supporting Information). Photoirradiation was performed using a photo-reactor with a broadband visible light source of  $400\text{--}700\ \text{nm}$  at different time intervals. The control samples were kept in the dark. The linear plots showed a gradual decrease of the intensity of the band indicating generation of singlet oxygen (Figure 5c). The diiodinated BODIPY complex **2** showed significant generation of  $^1\text{O}_2$  compared to the noniodinated complex **1** as evidenced from the higher slope signifying formation of more singlet oxygen (Figure 5c).

**Photoinduced Anticancer Activity.** The antitumor activity of the platinum complexes **1** and **2** along with their ligands was investigated on immortalized HaCaT human skin keratinocyte cells and MCF-7 human breast cancer cells in dark and light ( $400\text{--}700\ \text{nm}$ ) by MTT assay (Table 3, Figure 6, and

**Table 3.** Photocytotoxicity of the Complexes and the Ligands

compound	HaCaT ( $\mu\text{M}$ )		MCF-7 ( $\mu\text{M}$ )	
	IC <sub>50</sub> (light) <sup>a</sup>	IC <sub>50</sub> (dark) <sup>b</sup>	IC <sub>50</sub> (light) <sup>a</sup>	IC <sub>50</sub> (dark) <sup>b</sup>
<b>1</b>	$0.15 \pm 0.03$	$>80$	$6.7 \pm 0.8$	$>80$
<b>2</b>	$0.10 \pm 0.01$	$>65$	$2.6 \pm 0.1$	$>38$
$L^1$	$5.1 \pm 0.9$	$38.0 \pm 1.3$	$10.0 \pm 0.9$	$40.0 \pm 0.2$
$L^2$	$2.0 \pm 0.3$	$19.0 \pm 0.1$	$4.5 \pm 1.2$	$32 \pm 0.7$
[cisplatin] <sup>c</sup>		$3.2 \pm 0.3$		$69.7 \pm 1.2$

<sup>a</sup>IC<sub>50</sub> values ( $\mu\text{M}$ ) in the cells were for 4 h preincubation in the dark followed by 1 h exposure to visible light ( $400\text{--}700\ \text{nm}$ ; light dose =  $10\ \text{J cm}^{-2}$ , post incubation 19 h). <sup>b</sup>In dark with total 4 h incubation time. <sup>c</sup>IC<sub>50</sub> values from ref 13.

Figures S32 and S33, Supporting Information).<sup>47</sup> The PDT activity of complex **3** was not explored, as the complex does not have any photoactive moiety. Pyriplatin, a close analogue of imidazoplatin, is known to give an IC<sub>50</sub> value of  $109(\pm 10)\ \mu\text{M}$  in MCF-7 cells indicating its inactivity in the dark.<sup>14</sup>

The half maximal inhibitory concentrations (IC<sub>50</sub>) for complexes **1** and **2** in MCF-7 cells are  $6.7$  and  $2.6\ \mu\text{M}$ , respectively. The IC<sub>50</sub> value of the complexes for HaCaT cells is  $\sim 0.1\ \mu\text{M}$  in visible light ( $\lambda = 400\text{--}700\ \text{nm}$ , light dose =  $10\ \text{J cm}^{-2}$ ) with no noticeable toxicity in the dark (IC<sub>50</sub>  $> 80\ \mu\text{M}$ ). The MTT assay data reveal that platinum metal increases the photocytotoxicity by 34-fold for **1** and 20-fold for **2** compared to their free ligands in HaCaT cells in light, while being less toxic in the dark. The data compare well to that of the PDT drug Photofrin, which shows a similar difference in the IC<sub>50</sub> values in dark and light as observed for the MCF-7 cancer cells.

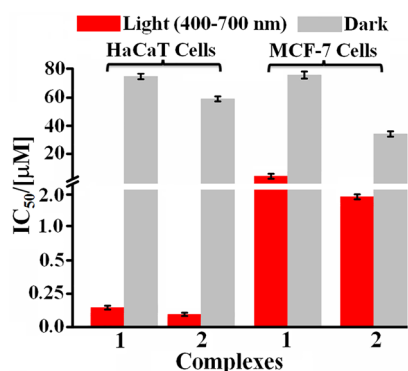


**Figure 6.** Photocytotoxicity of the complexes 1 and 2 in HaCaT and MCF-7 cells after 4 h incubation in dark followed by 1 h irradiation in visible light ( $\lambda = 400\text{--}700\text{ nm}$ ,  $10\text{ J cm}^{-2}$ , red bars). Gray bars correspond to samples unexposed to light.

**Mitochondrial Localization.** The emissive complex 1 was used for cellular imaging in 1% DMSO/DMEM buffer. DAPI as the nuclear staining dye and complex 1 ( $5\text{ }\mu\text{M}$ ) were treated with the HaCaT cells, followed by 4 h incubation in the dark, and subjected for confocal microscopy study. Complex 1 localized in the cytoplasm as evidenced from the merged images (Figure S34a, Supporting Information). MTR and ERTR were used for further study of subcellular colocalization. The overlay image of 1 with the MTR revealed preferential localization of the complex within the mitochondria (Figure 7a). The extent of colocalization was estimated by Pearson's correlation coefficient (PCC) method, which gave a value of 0.7 indicating significant mitochondrial localization of the complex (Figure S34b, Supporting Information).<sup>57</sup>

A partial overlap was observed when ERTR emission merged with the green emission of complex 1 (Figure 7b). The data suggest preferential localization of complex 1 into mitochondria than in endometrium reticulum (ER). Complex 2 for its nonemissive property was not used for the imaging study. The mitochondrial localization of the monofunctional platinum(II) complexes is of importance for dual activities that include (i) tumor organelle detection by imaging and (ii) PDT activity upon exposure to visible light. Interestingly, both the BODIPY complexes remain essentially nontoxic within the cells in darkness.

**Cellular ROS and Apoptosis.** DCFDA assay was done for detection of cellular ROS.<sup>58</sup> The nonfluorescent DCFDA is a cell-permeable dye that forms  $\text{H}_2\text{DCF}$  on enzymatic reaction and on oxidation by ROS generates fluorescent and cell membrane impermeable DCF dye. The apoptotic cell death upon visible light irradiation was studied for complexes 1 ( $0.2\text{ }\mu\text{M}$ ) and 2 ( $0.1\text{ }\mu\text{M}$ ) on incubation with the HaCaT cells in dark for 4 h followed by 1 h photoirradiation with visible light of  $400\text{--}700\text{ nm}$  in DPBS, and the assay was performed. A significant increase in the shift shown by 2 as compared to 1 upon light exposure suggests its higher ROS generation ability, while the ROS formation was insignificant in the dark (Figure S35, Supporting Information). The quantification of ROS in living cells was done using flow cytometric analysis by measuring the green fluorescence of DCF ( $\lambda_{\text{em}} = 525\text{ nm}$ ). The light-generated ROS is responsible for the cell death highlighting remarkable PDT activity of complex 2.

Annexin-V-FITC/PI assay was done to study the cell death by flow cytometry. The apoptotic cell death results in the flipping of the cell membrane. The red-emitting PI dye was used as a marker that intercalates with the DNA. Cells

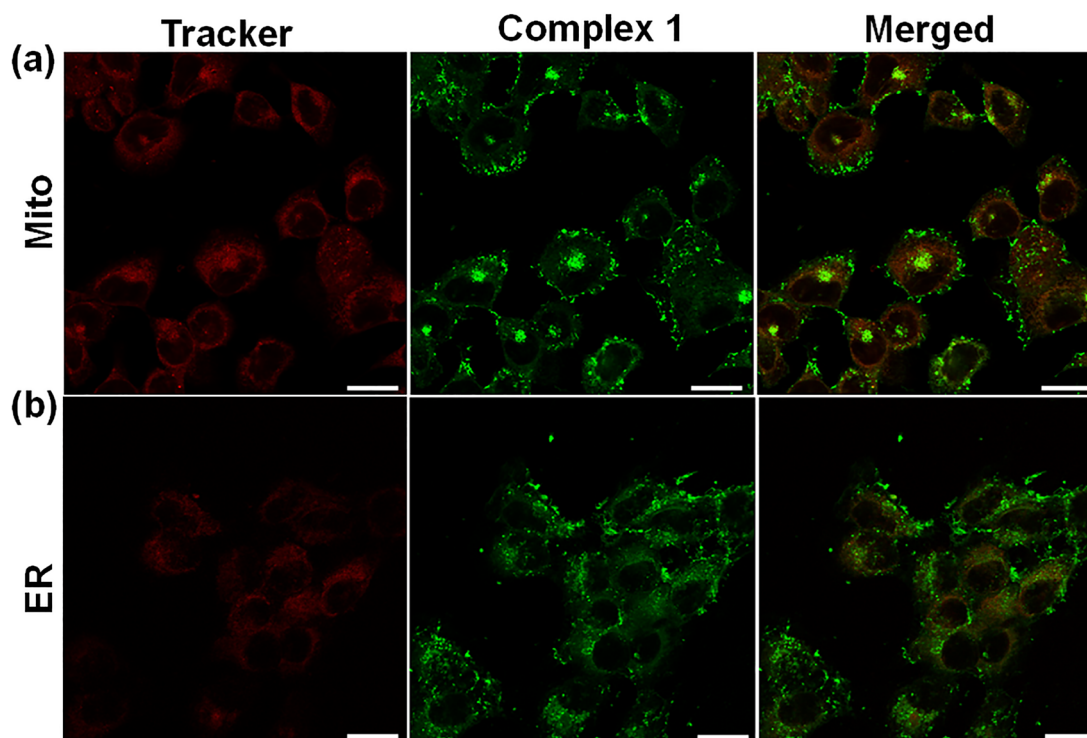


**Figure 7.** Confocal microscopic images of complex 1 ( $5\text{ }\mu\text{M}$ ) showing green emission in HaCaT cells on 4 h incubation in the dark. Top row is for MTR, and merged panels show significant mitochondrial localization of complex 1. Merged panel for ERTR in second panel (b) showed only partial localization of 1 in the ER. Scale bar =  $15\text{ }\mu\text{m}$ .

undergoing early apoptosis were identified as single positive population for FITC, while necrotic cell population was stained only by PI. The double positive population has cells that are in late apoptosis with compromised cell membrane. To study apoptotic cell death on light activation, HaCaT cells were treated with complexes 1 and 2 (0.2  $\mu\text{M}$ , 4 h incubation) followed by 1 h photoirradiation (400–700 nm). The assay was performed after 16 h post incubation period (Figure 8, Figures

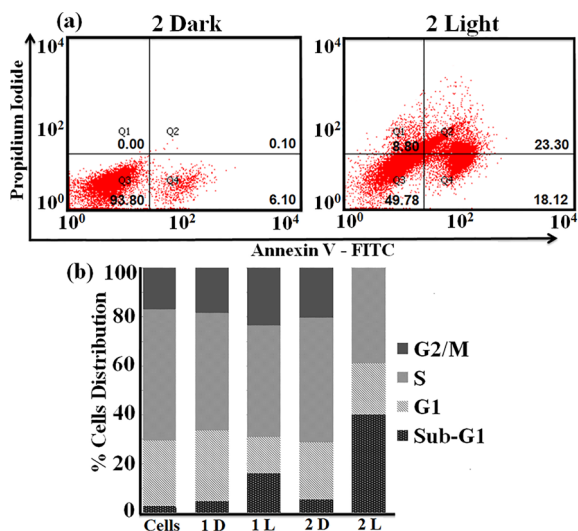


**Figure 8.** Annexin V-FITC/PI assay for apoptosis by FACS analysis in HaCaT cells with 4 h incubation of the complex (0.2  $\mu\text{M}$ ): (a) complex 2 in dark and light (1 h, 400–700 nm). The per cent cell population is shown in respective quadrants [lower left: live cells, lower right: early apoptotic cells, upper right: late apoptotic cells, and upper left: dead cells]. (b) The bar diagram shows per cent cell population in different phases of cell-cycle progression [D: in dark; L: on 1 h light exposure ( $\lambda = 400\text{--}700\text{ nm}$ )]. Errors are within  $\pm 3\%$ .

S36 and S37, Supporting Information). The cell cycle assays gave cellular apoptotic population by a low DNA content, where the DNA was stained with PI and quantified by FACS analysis. It showed  $\sim 41\%$  increase in the sub-G1 cell population

when treated with complex 2, whereas  $\sim 19\%$  for complex 1 upon photoirradiation (1 h,  $\lambda = 400\text{--}700\text{ nm}$ ) in HaCaT cells indicated higher generation of ROS. The statistical analysis of the histograms is shown in Figure 8b as a bar diagram (Figure S38, Supporting Information).

**9-Ethylguanine Binding.** Monofunctional platinum(II) complexes are known to form covalent adducts with nucleotide bases predominantly at the N7 position of guanosine and consequently do not unwind or bend the structure of the DNA duplex.<sup>59–63</sup> Unlike classical bifunctional platinum(II) complexes like cisplatin and its analogues, which induce distortion in DNA and inhibit cellular processes, monofunctional platinum(II) complexes show unconventional mode of action. Therefore, the formation of Pt(II)-DNA adduct was studied using 9-ethylguanine (9-EtG) as a model nucleobase by ESI-MS and <sup>1</sup>H NMR spectroscopy. The major peaks observed for 1 and 2 at *m/z* values of 831.25 and 1088.06 are assignable to the mono adducts, specifically,  $[\{\text{Pt}(\text{NH}_3)(\text{L}^1)\text{Cl}(9\text{-EtG})\} + \text{H}]^+$  and  $[\{\text{Pt}(\text{NH}_3)(\text{L}^2)\text{Cl}(9\text{-EtG}-\text{Li}^+)\}]^+$  (Figure 9).

Formation of  $[\text{Pt}(\text{NH}_3)(\text{L}^1)\text{Cl}(9\text{-EtG})]^+$  instead of the anticipated  $[\text{Pt}(\text{NH}_3)_2(\text{L})(9\text{-EtG})]^{2+}$  due to replacement of an ammine group instead of the bound chloride is of significance. The isotopic distribution pattern shown in Figure 9 unequivocally indicates the formation of unipositively charged platinum metal–guanosine adduct in both the complexes 1 and 2 with the separation of one mass unit from the adjacent peaks. The data suggest that one of the ammine group of the *cis*- $[\text{Pt}(\text{NH}_3)_2(\text{L})\text{Cl}]^+$  gets replaced instead of the chloride ligand. This could be due to higher *trans* effect of chloride ligand than ammonia in the noncellular medium (inset in Figure 10). Further investigation was done by <sup>1</sup>H NMR spectroscopy. Both the complexes were first treated with 9-EtG in a 1:3 molar ratio, followed by incubation in *d*<sub>6</sub>-DMSO–D<sub>2</sub>O mixture, and the reaction was monitored at different time intervals (Figure 10, Figures S39 and S40, Supporting Information).

The H8 proton of 9-EtG showed a downfield shift from 7.70 after 12 h of incubation implying that the platination site is at N7 position of the nucleobase. Two different peaks at 8.32 and 8.39 ppm in 2 and at 8.28 and 8.32 ppm in 1 of equal intensities were observed in <sup>1</sup>H NMR spectra suggesting the possibility of

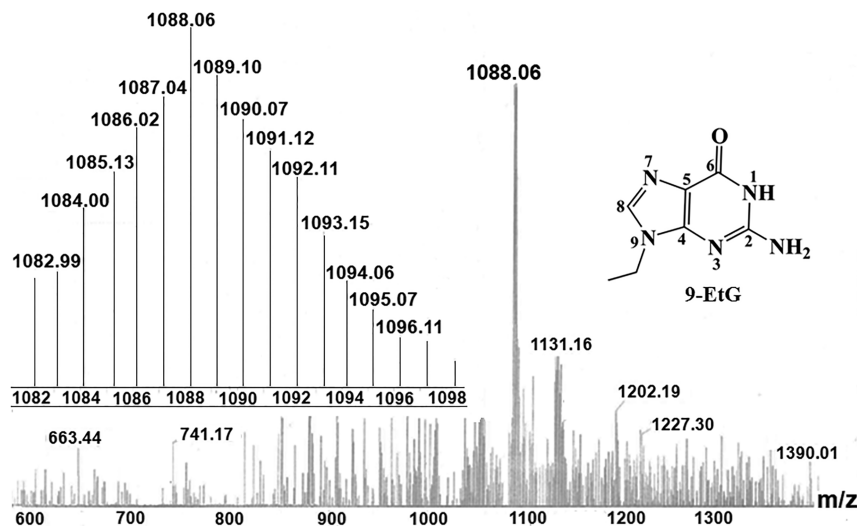


**Figure 9.** ESI-MS spectrum of complex 2 and 9-EtG (1:3 mol ratios) recorded in *d*<sub>6</sub>-DMSO–D<sub>2</sub>O mixture after incubation at 37 °C for 24 h. (inset) The isotopic distribution pattern indicated the presence of platinum in the DNA adduct. Assignments: 1088.06,  $[\{\text{Pt}(\text{NH}_3)(\text{L}^2)\text{Cl}(9\text{-EtG}-\text{Li}^+)\}]^+$  ( $\text{C}_{30}\text{H}_{32}\text{BClF}_2\text{LiN}_{10}\text{OPt}$ , calcd 1088.04).

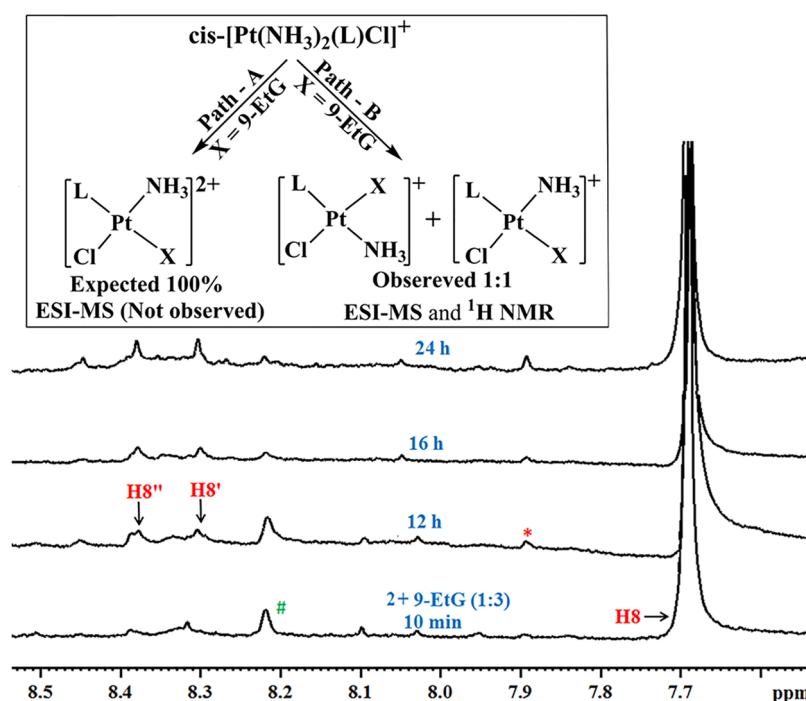


**Figure 10.** Stack plot of the aromatic region during the binding study of complex 2 with 9-EtG (1:3 molar ratio) in  $D_2O$ – $DMSO-d_6$  by  $^1H$  NMR, where \* indicates the signals of intact complex 2. A downfield shift of H8 proton (free 9-EtG) was observed as H8'/H8'' signals in 9-EtG bound to complex 2.

formation of both *cis* and *trans* adducts of formulation  $[Pt(NH_3)(L)Cl(9-EtG)]^+$  in a 1:1 molar ratio (shown as inset of Figure 10). The data obtained from the model studies suggest that the complexes are capable of forming Pt-DNA adduct.

Furthermore, the DNA binding ability of the cationic monofunctional platinum(II) complexes was studied by UV–visible and viscosity methods using calf thymus (ct) DNA at pH of 7.2 in Tris-HCl buffer (5 mM). Complexes 1 and 2 showed a gradual decrease in the absorption intensity upon increasing the concentration of ct-DNA and gave moderate DNA binding constant ( $K_b$ ) values (Table 1, Figures S41 and S42, Supporting Information). The DNA binding was further investigated by viscometric titrations in which  $(\eta/\eta_0)^{1/3}$  versus  $[complex]/[DNA]$  ratio was plotted. The results indicate intermediate binding of the complexes compared to DNA intercalator ethidium bromide (EB) and DNA minor groove binder Hoechst 33258 dye (Table 1, Figure S43a, Supporting Information). Thermal denaturation studies were performed to study any DNA cross-link formation. Intercalating molecules like EB enhance the stability of duplex DNA with a larger positive shift in the DNA melting temperature than groove binders like Hoechst dye. Complexes 1 and 2 showing low  $\Delta T_m$  values of  $\sim 2$  °C are likely to be covalently binding to DNA in preference to any intercalative mode of DNA binding (Table 1 and Figure S43b, Supporting Information).

## CONCLUSIONS

In conclusion, two imidazoplatin derivatives of formulation  $cis-[Pt(NH_3)_2(L)Cl](NO_3)$  of the N-donor imidazole ligand (L) having pendant fluorescent (in  $L^1$ ) and nonfluorescent (in  $L^2$ ) BODIPY moieties are prepared and characterized as new monofunctional platinum-based PDT agents. Complex 1 with a fluorescent ligand  $L^1$  is used for cellular imaging study, and this complex showed significant mitochondrial localization and

minor localization in the endoplasmic reticulum (ER). Targeting mitochondria is of importance, as this can circumvent the drawbacks associated with nuclear DNA binding bifunctional platinum drugs. The nuclear excision repair (NER) mechanism that operates for nuclear DNA is absent for the mitochondrial DNA. Again, ER stress causes cellular apoptosis. Complex 2 having a BODIPY moiety with two iodine atoms in  $L^2$  is an efficient photosensitizer, and the complex showed remarkable PDT activity in visible light with low  $IC_{50}$  values, while being less toxic in the dark. This highlights the utility of platinum-based photosensitizers as substitutes for organic macrocyclic PDT dyes like Photofrin and its analogues. The ROS involved in the PDT activity is found to be singlet oxygen ( $^1O_2$ ) with the nonfluorescent complex 2 generating it in higher quantity than the fluorescent complex 1. The present study established formation of Pt-DNA adducts involving the complexes and 9-EtG as a model substrate. The mechanistic pathway involves replacement of an ammine base instead of a chloride due to higher *trans*-effect of the chloride than ammine. Further biological studies are needed to understand the reaction pathway in a cellular medium. This work provides new insights and directions in the chemistry of monofunctional platinum(II) complexes that are close analogues to cisplatin. Such complexes with excellent anticancer activity on light activation akin to PDT effect of hematoporphyrin could act as potential substitutes of the toxic macrocyclic organic dyes.

## ASSOCIATED CONTENT

### Supporting Information

The Supporting Information is available free of charge on the ACS Publications website at DOI: 10.1021/acs.inorgchem.7b01346.

Experimental methods and measurements, reaction scheme, ESI-MS, NMR, IR spectra, UV–visible data,

cyclic voltammograms, stability study, unit-cell packing diagram of complex **3** and **L**<sup>1</sup>, optimized structure and frontier molecular orbitals, singlet oxygen generation, MTT assay, confocal imaging, DCFDA assay, FACS analysis, binding with 9-EtG, DNA binding by UV-vis, viscosity and thermal denaturation study, crystallographic parameters, bond distances/angles, and Cartesian coordinates of the complexes (PDF)

### Accession Codes

CCDC 1524705–1524706 contain the supplementary crystallographic data for this paper. These data can be obtained free of charge via [www.ccdc.cam.ac.uk/data\\_request/cif](http://www.ccdc.cam.ac.uk/data_request/cif), or by emailing [data\\_request@ccdc.cam.ac.uk](mailto:data_request@ccdc.cam.ac.uk), or by contacting The Cambridge Crystallographic Data Centre, 12 Union Road, Cambridge CB2 1EZ, UK; fax: +44 1223 336033.

### AUTHOR INFORMATION

#### Corresponding Authors

\*E-mail: [arc@ipc.iisc.ernet.in](mailto:arc@ipc.iisc.ernet.in) (A.R.C.)

\*E-mail: [paturu@mrdg.iisc.ernet.in](mailto:paturu@mrdg.iisc.ernet.in) (P.K.)

#### ORCID

Akhil R. Chakravarty: 0000-0002-6471-9167

#### Notes

The authors declare no competing financial interest.

### ACKNOWLEDGMENTS

The authors thank the Department of Science and Technology (DST), Government of India, for financial support (Grant Nos. SR/S5/MBD-02/2007 and EMR/2015/000742). The authors also thank the Alexander von Humboldt Foundation, Germany, for an electrochemical system. A.R.C. thanks the DST for J. C. Bose National Fellowship. P.K.'s research group is funded by DBT-IISc grants. M.K.R. thanks CSIR for his research fellowship. We thank Dr. Uttara, Urvashi and Deepika for FACS data, Saima and Santosh for confocal microscopy images, and Prof. A. Mukherjee of IISER-Kolkata for providing 9-ethylguanine.

### REFERENCES

- (1) Johnstone, T. C.; Suntharalingam, K.; Lippard, S. J. The Next Generation of Platinum Drugs: Targeted Pt(II) Agents, Nanoparticle Delivery and Pt(IV) Prodrugs. *Chem. Rev.* **2016**, *116*, 3436–3486.
- (2) Wilson, J. J.; Lippard, S. J. Synthetic Methods for the Preparation of Platinum Anticancer Complexes. *Chem. Rev.* **2014**, *114*, 4470–4495.
- (3) Mugge, C.; Marzo, T.; Massai, L.; Hildebrandt, J.; Ferraro, G.; Rivera-Fuentes, P.; Metzler-Nolte, N.; Merlino, A.; Messori, L.; Weigand, W. Platinum(II) Complexes with O,S Bidentate Ligands: Biophysical Characterization, Antiproliferative Activity and Crystallographic Evidence of Protein Binding. *Inorg. Chem.* **2015**, *54*, 8560–8570.
- (4) Dhar, S.; Gu, F. X.; Langer, R.; Farokhzad, O. C.; Lippard, S. J. Targeted Delivery of Cisplatin to Prostate Cancer Cells by Aptamer Functionalized Pt(IV) Prodrug-PLGA-PEG Nanoparticles. *Proc. Natl. Acad. Sci. U. S. A.* **2008**, *105*, 17356–17361.
- (5) Farrell, N. P. Multi-Platinum Anti-Cancer Agents. Substitution-Inert Compounds for Tumor Selectivity and New Targets. *Chem. Soc. Rev.* **2015**, *44*, 8773–8785.
- (6) White, J. D.; Haley, M. M.; DeRose, V. J. Multifunctional Pt(II) Reagents: Covalent Modifications of Pt Complexes Enable Diverse Structural Variation and In-Cell Detection. *Acc. Chem. Res.* **2016**, *49*, 56–66.
- (7) Wang, X.; Guo, Z. Targeting and Delivery of Platinum-Based Anticancer Drugs. *Chem. Soc. Rev.* **2013**, *42*, 202–224.
- (8) Patra, M.; Johnstone, T. C.; Suntharalingam, K.; Lippard, S. J. A Potent Glucose-Platinum Conjugate Exploits Glucose Transporters and Preferentially Accumulates in Cancer Cells. *Angew. Chem., Int. Ed.* **2016**, *55*, 2550–2554.
- (9) Basu, U.; Banik, B.; Wen, R.; Pathak, R. K.; Dhar, S. The Platin-X Series: Activation, Targeting, and Delivery. *Dalton Trans.* **2016**, *45*, 12992–13004.
- (10) Mackay, F. S.; Woods, J. A.; Heringová, P.; Kaspárková, J.; Pizarro, A. M.; Moggach, S. A.; Parsons, S.; Brabec, V.; Sadler, P. J. A Potent Cytotoxic Photoactivated Platinum Complex. *Proc. Natl. Acad. Sci. U. S. A.* **2007**, *104*, 20743–20748.
- (11) Farrer, N. J.; Woods, J. A.; Salassa, L.; Zhao, Y.; Robinson, K. S.; Clarkson, G.; Mackay, F. S.; Sadler, P. J. A Potent Trans-Diimine Platinum Anticancer Complex Photoactivated by Visible Light. *Angew. Chem., Int. Ed.* **2010**, *49*, 8905–8908.
- (12) Xue, X.; Zhu, C.; Chen, H.; Bai, Y.; Shi, X.; Jiao, Y.; Chen, Z.; Miao, Y.; He, W.; Guo, Z. A New Approach to Sensitize Antitumor Monofunctional Platinum(II) Complexes via Short Time Photo-Irradiation. *Inorg. Chem.* **2017**, *56*, 3754–3762.
- (13) Mitra, K.; Patil, S.; Kondaiah, P.; Chakravarty, A. R. 2-(Phenylazo)pyridine platinum(II) Catecholates Showing Photocytotoxicity, Nuclear uptake, and Glutathione-Triggered Ligand Release. *Inorg. Chem.* **2015**, *54*, 253–264.
- (14) Park, G. Y.; Wilson, J. J.; Song, Y.; Lippard, S. J. Phenanthriplatin, a Monofunctional DNA-Binding Platinum Anticancer Drug Candidate with Unusual Potency and Cellular Activity Profile. *Proc. Natl. Acad. Sci. U. S. A.* **2012**, *109*, 11987–11992.
- (15) Riddell, I. A.; Johnstone, T. C.; Park, G. Y.; Lippard, S. J. Nucleotide Binding Preference of the Monofunctional Platinum Anticancer-Agent Phenanthriplatin. *Chem. - Eur. J.* **2016**, *22*, 7574–7581.
- (16) Suryadi, J.; Bierbach, U. DNA Metalating-Intercalating Hybrid Agents for the Treatment of Chemoresistant Cancers. *Chem. - Eur. J.* **2012**, *18*, 12926–12934.
- (17) Malina, J.; Farrell, N. P.; Brabec, V. DNA Condensing Effects and Sequence Selectivity of DNA Binding of Antitumor Noncovalent Polynuclear Platinum Complexes. *Inorg. Chem.* **2014**, *53*, 1662–1671.
- (18) Johnstone, C.; Wilson, J. J.; Lippard, S. J. Monofunctional and Higher-Valent Platinum Anticancer Agents. *Inorg. Chem.* **2013**, *52*, 12234–12249.
- (19) Casini, A.; Reedijk, J. Interactions of Anticancer Pt Compounds with Proteins: An Overlooked Topic in Medicinal Inorganic Chemistry. *Chem. Sci.* **2012**, *3*, 3135–3144.
- (20) Wang, X.; Wang, X.; Guo, Z. Functionalization of Platinum Complexes for Biomedical Applications. *Acc. Chem. Res.* **2015**, *48*, 2622–2631.
- (21) Knoll, J. D.; Albani, B. A.; Turro, C. New Ru(II) Complexes for Dual Photoreactivity: Ligand Exchange and <sup>1</sup>O<sub>2</sub> Generation. *Acc. Chem. Res.* **2015**, *48*, 2280–2287.
- (22) Naik, A.; Rubbiani, R.; Gasser, G.; Spingler, B. Visible-Light-Induced Annihilation of Tumor Cells with Platinum-Porphyrin Conjugates. *Angew. Chem., Int. Ed.* **2014**, *53*, 6938–6941.
- (23) Schatzschneider, U. Photoactivated Biological Activity of Transition-Metal Complexes. *Eur. J. Inorg. Chem.* **2010**, 1451–1467.
- (24) Presa, A.; Brissos, R. F.; Caballero, A. B.; Borilovic, I.; Korrodi-Gregório, L.; Pérez-Tomás, R.; Roubeau, O.; Gamez, P. Photo-switching the Cytotoxic Properties of Platinum(II) Compounds. *Angew. Chem., Int. Ed.* **2015**, *54*, 4561–4565.
- (25) Mitra, K.; Gautam, S.; Kondaiah, P.; Chakravarty, A. R. The Cis-Diammineplatinum(II) Complex of Curcumin: A Dual Action DNA Crosslinking and Photochemotherapeutic Agent. *Angew. Chem., Int. Ed.* **2015**, *54*, 13989–13993.
- (26) Mari, C.; Pierroz, V.; Ferrari, S.; Gasser, G. Combination of Ru(II) Complexes and Light: New Frontiers in Cancer Therapy. *Chem. Sci.* **2015**, *6*, 2660–2686.
- (27) Banerjee, S.; Chakravarty, A. R. Metal Complexes of Curcumin for Cellular Imaging, Targeting, and Photoinduced Anticancer Activity. *Acc. Chem. Res.* **2015**, *48*, 2075–2083.

- (28) Raza, M. K.; Mitra, K.; Shettar, A.; Basu, U.; Kondaiah, P.; Chakravarty, A. R. Photoactive Platinum(II)  $\beta$ -diketonates as Dual Action Anticancer Agents. *Dalton Trans.* **2016**, *45*, 13234–13243.
- (29) Turan, I. S.; Yildiz, D.; Turksay, A.; Gunaydin, G.; Akkaya, E. U. A Bifunctional Photosensitizer for Enhanced Fractional Photodynamic Therapy: Singlet Oxygen Generation in the Presence and Absence of Light. *Angew. Chem., Int. Ed.* **2016**, *55*, 2875–2878.
- (30) Velema, W. A.; Szymanski, W.; Feringa, B. L. Photopharmacology: Beyond Proof of Principle. *J. Am. Chem. Soc.* **2014**, *136*, 2178–2191.
- (31) Lovell, J. F.; Liu, T. W. B.; Chen, J.; Zheng, G. Activable Photosensitizers for Imaging and Therapy. *Chem. Rev.* **2010**, *110*, 2839–2857.
- (32) Dąbrowski, J. M.; Arnaut, L. G. Photodynamic Therapy (PDT) of Cancer: From Local to Systemic Treatment. *Photochem. Photobiol. Sci.* **2015**, *14*, 1765–1780.
- (33) Renfrew, A. K.; Bryce, N. S.; Hambley, T. Cobalt(III) Chaperone Complexes of Curcumin: Photoreduction, Cellular Accumulation and Light-Selective Toxicity towards Tumour Cells. *Chem. - Eur. J.* **2015**, *21*, 15224–15234.
- (34) Castano, A. P.; Mroz, P.; Hamblin, M. R. Photodynamic Therapy and Anti-Tumor Immunity. *Nat. Rev. Cancer* **2006**, *6*, 535–545.
- (35) Basu, U.; Khan, I.; Hussain, A.; Kondaiah, P.; Chakravarty, A. R. Photodynamic Effect in Near-IR Light by a Photocytotoxic Iron(III) Cellular Imaging Agent. *Angew. Chem., Int. Ed.* **2012**, *51*, 2658–2661.
- (36) Zhu, Z.; Wang, X.; Li, Y.; Aime, S.; Sadler, P. J.; Guo, Z. Platinum(II)-Gadolinium(III) Complexes as Potential Single-Molecular Theranostic Agents for Cancer Treatment. *Angew. Chem., Int. Ed.* **2014**, *53*, 13225–13228.
- (37) Oliveira, V. A.; Iglesias, B. A.; Auras, B. L.; Neves, A.; Terenzi, H. Photoactive Meso-tetra(4-Pyridyl)porphyrin-Tetrakis-[chloro-(2,2'-bipyridine)platinum(II) Derivatives Recognize and Cleave DNA upon Irradiation. *Dalton Trans.* **2017**, *46*, 1660–1669.
- (38) Mao, J.; Zhang, Y.; Zhu, J.; Zhang, C.; Guo, Z. Molecular Combo of Photodynamic Therapeutic Agent Silicon(IV) Phthalocyanine and Anticancer Drug Cisplatin. *Chem. Commun.* **2009**, *8*, 908–910.
- (39) Doherty, R. E.; Sazanovich, I. V.; McKenzie, L. K.; Stasheuski, A. S.; Coyle, R.; Baggaley, E.; Bottomley, S.; Weinstein, J. A.; Bryant, H. E. Photodynamic killing of Cancer Cells by a Platinum(II) complex with Cyclometallating Ligand. *Sci. Rep.* **2016**, *6*, 22668.
- (40) Sun, T.; Guan, X.; Zheng, M.; Jing, X.; Xie, Z. Mitochondria-Localized Fluorescent BODIPY-Platinum Conjugate. *ACS Med. Chem. Lett.* **2015**, *6*, 430–433.
- (41) Miller, M. A.; Askevold, B.; Yang, K. S.; Kohler, R. H.; Weissleder, R. Platinum Compounds for High-Resolution in Vivo Cancer Imaging. *ChemMedChem* **2014**, *9*, 1131–1135.
- (42) Mitra, K.; Gautam, S.; Kondaiah, P.; Chakravarty, A. R. BODIPY-Appended 2-(2-Pyridyl)benzimidazole Platinum(II) Catecholates for Mitochondria-Targeted Photocytotoxicity. *ChemMedChem* **2016**, *11*, 1956–1967.
- (43) Michel, B. W.; Lippert, A. R.; Chang, C. J. A Reaction-Based Fluorescent Probe for Selective Imaging of Carbon Monoxide in Living Cells Using a Palladium-Mediated Carbonylation. *J. Am. Chem. Soc.* **2012**, *134*, 15668–15671.
- (44) Walker, N.; Stuart, D. An Empirical Method for Correcting Diffractometer Data for Absorption Effects. *Acta Crystallogr., Sect. A: Found. Crystallogr.* **1983**, *39*, 158–166.
- (45) Sheldrick, G. M. Crystal Structure Refinement with SHELXL. *Acta Crystallogr., Sect. C: Struct. Chem.* **2015**, *71*, 3–8.
- (46) Farrugia, L. J. WinGX and ORTEP for Windows: an update. *J. Appl. Crystallogr.* **2012**, *45*, 849–854.
- (47) Skehan, P.; Storeng, R.; Scudiero, D.; Monks, A.; McMahon, J.; Vistica, D.; Warren, J. T.; Bokesch, H.; Kenney, S.; Boyd, M. R. New Colorimetric Cytotoxicity Assay for Anticancer-Drug Screening. *J. Natl. Cancer Inst.* **1990**, *82*, 1107–1112.
- (48) Ulrich, G.; Ziesel, R. Convenient and Efficient Synthesis of Functionalized Oligopyridine Ligands Bearing Accessory Pyromethene-BF<sub>2</sub> Fluorophores. *J. Org. Chem.* **2004**, *69*, 2070–2083.
- (49) Guliyev, F.; Ozturk, S.; Sahin, E.; Akkaya, E. U. Expanded Bodipy Dyes: Anion Sensing Using a Bodipy Analog with an Additional Difluoroboron Bridge. *Org. Lett.* **2012**, *14*, 1528–1531.
- (50) Liu, Q. X.; Xu, F. B.; Li, Q. S.; Zeng, X. S.; Leng, X. B.; Chou, Y. L.; Zhang, Z. Z. A Luminescent silver(I) Carbene Stair Polymer. *Organometallics* **2003**, *22*, 309–314.
- (51) Bhattacharyya, A.; Dixit, A.; Mitra, K.; Banerjee, S.; Karande, A.; Chakravarty, A. R. BODIPY Appended Copper(II) Complexes of Curcumin Showing Mitochondria Targeted Remarkable Photocytotoxicity in Visible Light. *MedChemComm* **2015**, *6*, 846–851.
- (52) Johnston, D. H.; Miller, N. A.; Tackett, C. B. cis-Diamminedichloridoplatinum(II) N,N-dimethylformamide monosolvate. *Acta Crystallogr., Sect. E: Struct. Rep. Online* **2012**, *68*, m863–m64.
- (53) Frisch, M. J. *Gaussian 09*, revision A.1; Gaussian, Inc.: Wallingford, CT, 2009; see [Supporting Information](#) for full citation.
- (54) Becke, A. D. Density-Functional Exchange-Energy Approximation with Correct Asymptotic Behavior. *Phys. Rev. A: At., Mol., Opt. Phys.* **1988**, *38*, 3098–3100.
- (55) Becke, A. D. Density-Functional Thermochemistry. III. The Role of Exact Exchange. *J. Chem. Phys.* **1993**, *98*, 5648–5652.
- (56) Bartosz, G. Use of Spectroscopic Probes for Detection of Reactive Oxygen Species. *Clin. Chim. Acta* **2006**, *368*, 53–76.
- (57) Dunn, K. W.; Kamocka, M. M.; McDonald, H. J. A Practical Guide to Evaluating Colocalization in Biological Microscopy. *Am. J. Physiol. Cell Physiol.* **2011**, *300*, C723–C742.
- (58) Wang, H.; Joseph, J. A. Quantifying cellular oxidative stress by dichlorofluorescein assay using microplate reader. *Free Radical Biol. Med.* **1999**, *27*, 612–616.
- (59) Reedijk, J. Improved Understanding in Platinum Antitumor Chemistry. *Chem. Commun.* **1996**, 801–806.
- (60) Pizarro, A. M.; Sadler, P. J. Unusual DNA binding modes for metal anticancer complexes. *Biochimie* **2009**, *91*, 1198–1211.
- (61) Karmakar, S.; Purkait, K.; Chatterjee, S.; Mukherjee, A. Anticancer activity of a cis-dichloridoplatinum(II) complex of a chelating nitrogen mustard: insight into unusual guanine binding mode and low deactivation by glutathione. *Dalton Trans.* **2016**, *45*, 3599–3615.
- (62) Müller, B.; Shen, W. Z.; Sanz Miguel, P. J.; Albertí, F. M.; Van Der Wijst, T.; Noguera, M.; Rodríguez-Santiago, L.; Sodupe, M.; Lippert, M. Pt(II) Coordination to N1 of 9-Methylguanine: Why It Facilitates Binding of Additional Metal Ions to the Purine Ring. *Chem. - Eur. J.* **2011**, *17*, 9970–9983.
- (63) Wu, S.; Wang, X.; Zhu, C.; Song, Y.; Wang, J.; Li, Y.; Guo, Z. Monofunctional Platinum Complexes Containing a 4-nitrobenzo-2-oxa-1,3-diazole Fluorophore: Distribution in Tumour Cells. *Dalton Trans.* **2011**, *40*, 10376–10382.